

Surface Photometry of Early-type Galaxies in the Hubble Deep Field

G. Fasano¹, M. Filippi², F. Bertola²

¹Astronomical Observatory of Padova, Vicolo dell' Osservatorio 5, 35122 Padova, Italy

²Department of Astronomy of the Padova University, Vicolo dell' Osservatorio 5, 35122 Padova, Italy
e-mail gfasano@leda.pd.astro.it

Received: September 1997. Accepted: November 1997

Abstract.

The detailed surface photometry of a sample of early-type galaxies in the Hubble Deep Field is presented as part of a long-term project aimed to settle strong observational constraints to the theories modelling the evolution of elliptical galaxies from the early stages.

The sample has been extracted, in the V_{606} band, from the database provided by the *ESO-STECF-HDF* Group (Couch 1996). The selection criteria involve the total magnitude, the number of pixels detected above the background level and an automatic star/galaxy classifier. Moreover, form visual inspection of the frames, we excluded the galaxies showing unambiguous late-type morphology. The analysis of the luminosity and geometrical profiles, carried out on the 162 candidates obeying our selection criteria, resulted in a list of 99 '*bona fide*' early-type galaxies, for which accurate total magnitudes and effective radii were computed on the basis of the equivalent luminosity profiles. The comparison with the magnitudes given by Williams et al.(1996) indicates that the automated photometry tends to underestimate the total luminosity of the ellipticals.

The luminosity profiles of most of galaxies in our sample follow fairly well the de Vaucouleurs law ('Normal' profiles). However, a relevant fraction of galaxies, even following the $r^{1/4}$ law in the main body light distribution, exhibit in the inner region a flattening of the luminosity profile not attributable to the *PSF* ('Flat' profiles) or, in some cases, a complex (multi-nucleus) structure ('Merger' profiles). A statistically significant correlation is found between the shapes of the luminosity profiles and the ellipticity distribution. In particular, the average ellipticity of galaxies belonging to the 'Flat' and 'Merger' classes is significantly higher than that of the 'Normal' galaxies. Finally, even taken into account the relevant uncertainty of the outer position angle profiles, the amount of isophotal twisting of HDF ellipticals turns out to be significantly larger with respect to that of the local samples.

Key words: Galaxies: elliptical and lenticular, Galaxies: fundamental parameters, Galaxies: photometry

Send offprint requests to: G. Fasano

1. Introduction

Understanding the processes governing the formation and the evolution of galaxies from the early stages is one of the major goals of the present day cosmology. Comprehensive numerical codes, linked with powerful CPU capabilities, make now possible to follow the evolution of primordial density fluctuations down to the stages preceding the formation of real galaxies (see Jenkins et al. 1997 for a recent review). White (1997) has also shown that the scaling relations expected after evolution of proto-galaxies of different morphologies seem to be in good agreement with those observed today, i.e. the Tully-Fisher (1977) and the Fundamental Plane (Dressler et al. 1987; Djorgovski & Davis 1987) relations.

Still, a number of key questions remain to be answered. We mention (among the others) the following ones: which is the parameter driving galaxies towards different morphologies? Are elliptical galaxies originated from gravitational collapse of primordial fluctuations (single burst of star formation whose duration depends on the onset of galactic winds) or are they the result of multiple merging (infall and recursive bursts)? Which is the influence of the internal and intergalactic absorption in determining the observed brightness and color profiles of high redshift galaxies?

Besides the global approach to the star formation history (Madau et al. 1997), answering these questions also requires detailed morphological and dynamical studies of galaxies in the early evolutionary stages. In particular, luminosity and geometrical profiles in different bands are needed to obtain unambiguous morphological classifications as well as reliable estimates of the galaxy sizes at intermediate and high redshifts.

Recent advances in the sensitivity and resolution of the observations both in imaging and spectroscopy with the *Hubble Space Telescope* (HST) and from the ground have greatly enlarged the horizon of morphological and dynamical studies for high redshift galaxies (Giavalisco et al. 1996, van Dokkum and Franx 1996, Shadé et al. 1996, Shadé et al. 1997, Oemler et al. 1997, Lowenthal et al. 1997, Pettini et al. 1997 and references therein). The Hubble Deep Field (HDF) is perhaps the most impressive example of these progresses (Ellis 1997).

The HDF project (Williams et al. 1996) has been realized using observational procedures (*dithering*) and data handling techniques (*drizzling*) aimed to improve not only the cosmetic of the final images, but also the resolution performances. In particular, after '*drizzling*', the pixel size in arcseconds of the three WF cameras turns out to be even better than that of the PC ($\sim 0''.040$ vs. $\sim 0''.046$). Moreover, the very long total exposure times of the final images allow to overcome the main limitation of the WFPC data, that is the relatively high surface brightness level usually reached for extended sources. This makes the HDF frames particularly suited in order to perform the detailed surface photometry of objects whose surface luminosity slowly decreases outwards down to very faint levels, as in the case of elliptical galaxies. We can rightfully assert that the HDF represents the best opportunity we had since now to study the morphology of elliptical galaxies at very high redshifts.

We have undertaken a long-term project aimed to produce the detailed surface photometry, in different bands, for a sample of early-type galaxies in the HDF. The main scientific goal of this project is to settle strong observational constraints to the theories modelling the evolution of elliptical galaxies from the early stages (e.g. Tantalo et al. 1996, Kauffmann and Charlot 1997, Chiosi et al. 1997 and references therein).

In this paper we present the surface photometry in the V_{606} band. In the forthcoming papers (Filippi et al. 1997, Fasano et al. 1997) we will present the surface photometry in the remaining 3 bands and discuss the improvements that the morphological information, together with the photometry in different optical and infrared bands, can produce in understanding the processes of galaxy formation and evolution.

In Section 2 we discuss the sample selection. Section 3 illustrates the techniques we used to extract the morphological information from the HDF frames. In Section 4 we present the results of the detailed surface photometry and discuss the global morphological properties of the sample.

2. Sample selection

Our sample of *early-type* galaxies has been extracted from the second release of the WFPC2-HDF frames, in the V_{606} band. Due to the efficiency curve of the WFPC2, this filter usually ensures a better S/N ratio with respect to the other available filters (U_{300} , B_{450} and I_{814}) even in the case of high redshift galaxies, as we verified by comparing the V_{606} and I_{814} images.

2.1. Selection criteria

The sample selection is based on the compilation provided by the *ESO-STECF-HDF* Group, obtained through the automated SExtractor algorithm (Bertin and Arnouts 1996). Among the other things, the catalog includes, for each object in the field, the total V_{606} magnitude in the STMAG system, the number of pixels (N_{pix}) detected above the background using a threshold of 1.3σ of the noise, and a star/galaxy (s/g) classifier, ranging from 0 to 1, which gives the probability that the object is stellar ($s/g=1$ means 'star'). After a preliminar inspection of the frames, supplemented by several fast average-tracing luminosity profiles of faint and/or small objects, we decided to set the following limits for inclusion in our preliminar sample: (1) $V_{606}(\text{STMAG}) \leq 26.5$; (2) $N_{pix} \geq 200$; (3) $(s/g) \leq 0.6$.

As for the first two limits, they concern essentially the technical '*feasibility*' of the morphological analysis. Although at

this stage we preferred not to be too much severe in the selection, these limits provide completeness criteria to our sample. The choice of the third limit turned out not to be critical, probably due to the very shape of the star profiles. Nevertheless, in this case we preferred to be more conservative, in order to prevent the inclusion of stars in our sample.

2.2. Morphological screening

We found 372 objects of the SExtractor catalog matching the above limits in the three chips of the WFC (the catalog does not include the PC). 29 objects from the chip #1 (PC) were added later to this list by simple visual inspection, so that the total preliminar sample turned out to be of 401 objects.

We used the '*imexam*' IRAF's tool, together with the '*Saoimage*' display facility, to estimate the morphological type of each object, thus producing a first screening of the galaxies in the sample. Apart from some cases, the angular resolution did not allow us to give precise Hubble types. Moreover, many faint galaxies appear heavily disturbed by the presence of close (often multiple) companions or peculiar structures, which obviously make even more difficult the classification. Nevertheless, most of the '*early-type*' candidates turned out to be easily recognizable on the basis of the light concentration. The dubious cases (mainly *S0s* and *Sa* galaxies) were retained at this stage and were examined later in a quantitative way (see next Section).

After this selection we were left with 134 galaxies. In order to check the reliability of our classifications, we compared them with those given by Van den Bergh et al.(1996) and by Statler(1996, private communication). Due to the different selection criteria, the three samples do not overlap exactly each other. Nevertheless, for the common objects the agreement was fairly good (80% with Van den Bergh et al. and 84% with Statler). To be more accurate, we decided to provisionally include in our sample all galaxies matching our selection criteria which, contrary to our estimates, were classified as '*early-type*' by Van den Bergh et al.(1996) and/or by Statler(1996). In this way 28 more galaxies enriched our sample, which become of 162 objects.

2.3. Final sample

We performed the detailed surface photometry of this sample, producing luminosity and geometrical profiles of each object. The next Section outlines the techniques we used to extract the morphological information from this very peculiar observational material. From the analysis of the luminosity and geometrical profiles, 34 objects of the sample have been recognized to be '*disk-dominated*' objects (likely *Sa* galaxies), whereas 28 more objects showed peculiar or unclassifiable profiles. These galaxies were excluded from the final sample of '*bona fide*' early-type galaxies.

The final sample of 99 galaxies is reported in Table 1, where column (1) gives the FOCAS list identification (Williams et al. 1996), columns (2) and (3) the J2000 coordinates α and δ , column (4) our morphological classification, columns (5) the morphological type (if available) given by van den Bergh et al.(1996).

Table 1. The Sample

FOCAS-ID	Coordinates(2000)		Morphology		Lum.Prof.	$V_{606}^{Tot}(\Delta_m)$	r_e^{eq}	ε_e	ε_{max}	$\Delta\theta$
	α	δ	Our	V.d.Bergh	class	(STMAG)	(")			(°)
ID_4_942_0	36 ^m	39 ^s .43	12° 11 ["] .76	E	E	1	24.75(.33)	0.54	0.18	0.25
ID_4_926_2	36	39.56	12 13.83	m	p	3	25.36(.17)	0.19	0.04	0.17
ID_4_928_1	36	40.01	12 07.37	S0	E	1	23.61(.15)	0.36	0.10	0.19
ID_4_878_2	36	40.74	12 04.96	E	E	2	25.79(.19)	0.22	0.35	0.35
ID_4_878_11	36	40.96	12 05.31	E	Sap	2	23.66(.14)	0.22	0.12	0.14
ID_4_822_0	36	41.15	12 10.56	E	E	1	25.42(.27)	0.33	0.08	0.10
ID_4_858_13	36	41.25	12 03.07	E	E	1	25.18(.23)	0.15	0.14	0.19
ID_4_767_0	36	41.49	12 14.98	S0	E	2	25.16(.15)	0.19	0.36	0.39
ID_4_661_1	36	41.62	12 35.67	E	E	2	24.96(.17)	0.22	0.18	0.23
ID_4_639_1	36	41.71	12 38.75	E	Et?	1	25.12(.14)	0.17	0.08	0.16
ID_4_937_0	36	42.28	11 26.18	E	E	1	25.50(.19)	0.18	0.19	0.22
ID_1_95_0	36	42.38	13 19.36	E	-	1	25.03(.13)	0.13	0.28	0.30
ID_4_602_0	36	42.41	12 32.48	E	E	1	25.30(.18)	0.16	0.24	0.28
ID_4_804_0	36	42.53	11 50.01	E	Ep?	1	25.40(.16)	0.20	0.23	0.27
ID_4_774_3	36	42.78	11 54.28	E	-	1	25.95(.18)	0.14	0.20	0.21
ID_4_581_11	36	42.87	12 27.85	E/S0	-	1	25.77(.15)	0.14	0.19	0.25
ID_4_845_0	36	42.92	11 37.27	E	Sa	2	25.08(.16)	0.20	0.37	0.37
ID_4_554_1	36	43.13	12 28.11	Ep	Ep	2	25.58(.20)	0.17	0.29	0.33
ID_4_493_0	36	43.16	12 42.20	S0	E	1	23.26(.24)	0.44	0.33	0.33
ID_4_727_0	36	43.41	11 51.57	E	Ep?	2	23.43(.10)	0.21	0.49	0.48
ID_4_565_0	36	43.63	12 18.25	m	Sap	3	23.46(.12)	0.31	0.18	0.28
ID_4_744_0	36	43.80	11 42.88	E	-	1	22.33(.18)	0.63	0.12	0.16
ID_2_82_1	36	44.07	14 09.92	E	E/m	2	24.92(.15)	0.18	0.27	0.28
ID_4_752_1	36	44.38	11 33.20	E	-	1	22.97(.22)	0.90	0.18	0.18
ID_1_56_0	36	44.46	13 13.10	E	-	1	26.38(.19)	0.13	0.15	0.21
ID_4_579_0	36	44.74	11 57.05	E	E/*	1	25.53(.14)	0.13	0.06	0.09
ID_1_37_1	36	44.79	13 07.23	m	-	3	25.75(.18)	0.13	0.50	0.46
ID_2_163_0	36	45.29	14 07.03	E	-	1	25.94(.19)	0.18	0.25	0.26
ID_4_555_2	36	45.33	11 54.52	E/S0	E	1	24.79(.21)	0.32	0.17	0.24
ID_4_368_0	36	45.35	12 33.70	E/S0	-	1	26.07(.22)	0.24	0.26	0.25
ID_2_80_0	36	45.40	13 50.07	E	-	2	25.64(.18)	0.18	0.26	0.28
ID_1_100_0	36	45.52	13 29.97	E	-	1	26.37(.14)	0.13	0.12	0.29
ID_1_35_0	36	45.61	13 08.92	E	-	1	24.35(.16)	0.21	0.24	0.26
ID_4_516_0	36	45.65	11 53.97	E	Et	1	25.30(.15)	0.18	0.13	0.20
ID_4_497_0	36	45.73	11 57.31	E	-	1	26.05(.17)	0.13	0.12	0.14
ID_4_520_0	36	45.79	11 50.52	E/S0	-	1	26.07(.19)	0.14	0.11	0.18
ID_2_61_0	36	46.12	13 34.62	E	E	2	25.91(.15)	0.15	0.26	0.31
ID_4_254_0	36	46.13	12 46.50	E	E/*	1	23.64(.19)	0.55	0.27	0.17
ID_1_47_0	36	46.16	13 13.89	E	-	2	25.17(.13)	0.15	0.38	0.37
ID_4_322_2	36	46.21	12 28.43	E	Et	2	25.59(.16)	0.16	0.23	0.28
ID_2_251_0	36	46.34	14 04.62	E/S0	-	1	22.96(.17)	0.52	0.05	0.14
ID_4_471_0	36	46.51	11 51.32	E	E	1	23.11(.07)	0.22	0.08	0.12
ID_4_289_0	36	46.95	12 26.08	E	E	1	25.73(.14)	0.16	0.11	0.20
ID_2_201_0	36	47.18	13 41.82	E	Et	1	24.45(.16)	0.14	0.15	0.24
ID_2_272_0	36	47.68	13 51.28	E	-	2	25.98(.16)	0.17	0.26	0.28
ID_2_363_0	36	47.71	14 09.43	E	-	2	25.94(.15)	0.15	0.25	0.33
ID_2_121_111	36	48.08	13 09.02	S0	-	1	21.48(.11)	0.60	0.04	0.23
ID_2_412_11	36	48.11	14 14.42	E/S0	Sap	2	25.42(.22)	0.17	0.27	0.42
ID_4_260_112	36	48.12	12 14.90	E	E	2	25.08(.13)	0.18	0.30	0.28
ID_2_449_1	36	48.34	14 16.63	E	E	2	24.11(.22)	0.22	0.24	0.30
ID_2_173_0	36	48.47	13 16.62	E	E	2	23.74(.29)	0.72	0.18	0.35
ID_2_537_12	36	48.71	14 22.62	E	Et	2	25.60(.15)	0.20	0.32	0.35
ID_3_51_0	36	48.72	13 02.45	E	E/*	1	25.93(.17)	0.17	0.08	0.14
ID_2_236_2	36	48.97	13 21.88	E	Et	1	24.81(.10)	0.16	0.03	0.13
ID_2_180_0	36	49.05	13 09.64	E	Sa	2	24.65(.15)	0.20	0.50	0.47
ID_4_274_0	36	49.11	11 50.54	S0	-	2	26.02(.25)	0.17	0.23	0.24
ID_2_264_2	36	49.38	13 11.22	E	E	1	22.80(.11)	0.21	0.24	0.26
ID_2_456_1111	36	49.44	13 46.88	S0	-	1	18.93(.05)	0.52	0.37	0.39
ID_3_229_0	36	49.48	12 48.73	E	E/*	2	24.96(.24)	0.24	0.10	0.12
ID_2_590_1	36	49.51	14 21.10	E	-	2	25.89(.21)	0.16	0.18	0.16
ID_4_109_0	36	49.60	12 12.68	E	p	2	25.29(.12)	0.16	0.38	0.40
ID_3_143_0	36	49.64	12 57.43	m	Sap	3	22.85(.15)	0.32	0.55	0.65

Table 1. ...continue...

FOCAS-ID	Coordinates(2000)		Morphology		Lum.Prof.	$V_{606}^{Tot}(\Delta_m)$	r_e^{eq}	ε_e	ε_{max}	$\Delta\theta$
	α	δ	Our	V.d.Bergh	class	(<i>STMAG</i>)	($''$)			($^{\circ}$)
ID_3.243_0	36 49.81	12 48.79	E/S0p	Ep	1	25.52(.21)	0.21	0.32	0.34	14
ID_2.456_22	36 50.03	13 51.99	S0	Ep	1	25.15(.12)	0.17	0.36	0.50	6
ID_3.321_1	36 50.27	12 45.75	S0	—	1	23.05(.13)	0.43	0.34	0.36	5
ID_2.373_0	36 50.30	13 29.73	E	E	1	25.58(.18)	0.16	0.27	0.33	9
ID_2.725_0	36 50.56	14 28.47	E	E	2	25.50(.15)	0.17	0.52	0.44	12
ID_2.693_1	36 51.35	14 11.02	E	E	2	25.22(.15)	0.18	0.18	0.25	22
ID_3.659_2	36 51.44	12 20.71	Ep	E/S0	1	25.69(.15)	0.13	0.18	0.17	23
ID_3.902_1	36 51.79	11 57.81	E/Sa	—	2	26.25(.22)	0.16	0.18	0.20	42
ID_2.531_0	36 51.97	13 32.18	E	E	3	24.06(.15)	0.29	0.10	0.07	15
ID_3.586_0	36 52.10	12 26.31	E	E/Sa	1	25.77(.36)	0.36	0.14	0.19	20
ID_2.646_0	36 52.23	13 48.07	E	E	2	25.14(.21)	0.20	0.42	0.38	5
ID_2.849_0	36 52.40	14 20.95	E	Ep	2	25.60(.26)	0.19	0.32	0.30	15
ID_3.625_0	36 52.51	12 24.78	m	p	3	25.39(.13)	0.15	0.50	0.49	3
ID_3.696_0	36 52.69	12 19.72	E	E	2	23.77(.09)	0.19	0.46	0.45	10
ID_2.637_0	36 52.76	13 39.08	E	E/*	1	25.18(.15)	0.18	0.11	0.14	80
ID_3.886_0	36 52.92	12 03.11	E	E	2	25.21(.18)	0.14	0.16	0.21	8
ID_2.726_1	36 53.12	13 46.25	E	—	1	26.75(.19)	0.11	0.23	0.18	35
ID_2.635_0	36 53.15	13 31.66	E	—	1	25.99(.15)	0.17	0.24	0.24	29
ID_2.591_2	36 53.18	13 22.75	E	—	2	25.05(.15)	0.18	0.31	0.30	10
ID_3.670_1	36 53.26	12 22.74	E	E	2	25.73(.21)	0.14	0.28	0.26	20
ID_2.643_0	36 53.42	13 29.52	m	E+E	3	25.03(.17)	0.22	0.65	0.62	5
ID_2.973_2	36 54.50	14 08.16	E	—	2	25.88(.18)	0.18	0.23	0.19	10
ID_3.118_1	36 54.73	13 14.73	E	E/*	1	24.59(.17)	0.14	0.08	0.09	10
ID_2.898_0	36 54.78	13 50.74	m	Sa	3	25.14(.20)	0.27	0.49	0.50	3
ID_3.743_0	36 54.95	12 21.44	E	—	2	25.61(.20)	0.19	0.11	0.14	93
ID_3.266_0	36 55.16	13 03.60	E	E	1	25.19(.19)	0.22	0.30	0.31	3
ID_3.180_1	36 55.46	13 11.19	E/S0	E	1	23.94(.21)	0.51	0.18	0.19	70
ID_2.966_0	36 55.77	13 48.78	E	E	2	25.83(.19)	0.18	0.24	0.24	40
ID_3.904_0	36 55.95	12 10.72	E	E	1	25.11(.13)	0.17	0.08	0.14	70
ID_3.815_1	36 56.65	12 20.12	E/S0	E	1	24.29(.20)	0.41	0.21	0.22	11
ID_3.355_0	36 56.92	13 01.56	E	E	1	24.16(.20)	0.39	0.04	0.08	5
ID_3.726_0	36 58.53	12 33.59	E	—	2	26.15(.18)	0.18	0.29	0.28	12
ID_3.363_1	36 58.57	13 05.47	E	—	1	26.23(.20)	0.11	0.05	0.04	5
ID_3.813_0	36 59.24	12 27.29	E	—	1	26.02(.18)	0.17	0.04	0.08	135
ID_3.748_0	36 59.98	12 35.95	E	—	1	26.23(.17)	0.15	0.23	0.20	16
ID_3.888_1	37 00.52	12 25.81	E	Sap	1	25.57(.18)	0.17	0.12	0.18	42
ID_3.790_1	37 00.56	12 34.60	E	—	2	22.60(.14)	0.40	0.10	0.13	20

3. Detailed surface photometry

The detailed surface photometry of our sample of HDF ellipticals in the V_{606} band was performed using the AIAP package (Fasano 1990), which is equipped with a completely interactive graphical interface, allowing flexible tools for sky subtraction, drawing, masking and fitting of the isophotes, PSF evaluation, etc. These capabilities, as well as the allowance for checking 'on-line' all steps of the procedure, turn out to be particularly useful when handling morphologically complex structures and/or closely interacting objects, a situation quite common in the case of the HDF galaxies.

Our magnitudes are given in the *STMAG* system.

3.1. Basic procedures

The second release of the HDF provided us with frames 'ready to be used', in the sense that all the standard reduction procedures (flat fielding, bias and dark-current removal, etc.), as

well as the specific ones (drizzling, position weighting, etc.), were already performed and the proper (constant) sky background was subtracted from each frame.

Nevertheless, since not negligible and systematic residuals in the backgrounds were detected, we decided to perform for each galaxy a '*local*' refinement of the background subtraction by linear interpolation of the residuals. After this refinement the mean (systematic) background variations were estimated to be of the order of $\sim 0.5\%$ of the original sky levels. These systematic variations have been used to estimate error bars in the outer luminosity and geometrical profiles of each object (see next subsection).

The isophotes were drawn with a fixed surface brightness step of $0^m.2$. Therefore, at least in the inner part of galaxies having steep luminosity profiles, isophotes might be oversampled, since the difference of radius between two successive isophotes might be lower than the pixelsize. We note, however, that the shapes of luminosity profiles are not modified

by the oversampling and that, whenever we introduce luminosity profiles weighting (i.e. fitting with analytical functions and extrapolation), we set to zero the weight of oversampled isophotes.

Low surface brightness isophotes (usually $\mu_{606} \geq 25^m.8$) were drawn after rebinning of the frames. The AIAP package allows to decide interactively when and how perform the rebinning, depending on the noise of each isophote. The maximum reachable surface brightness was not the same for all galaxies. It essentially turned out to depend on the presence of close companions and/or irregular sub-structures which often make useless to go much deep in drawing the isophotes. We can reach easily the surface brightness level of $28^m.0$. In the most favourable cases we were able to reach $\mu_{606} = 28^m.8$.

The isophotes of HDF ellipticals are often quite irregular due to the intrinsic complexity of the structures (which is likely to increase at increasing redshift), as well as to the presence of close (possibly interacting) companions. Therefore, the flexibility of the AIAP masking and ellipse fitting tools turned out to be useful in order to secure reliable profiles even for very intriguing cases. We mention, among the other things, the possibility to take fixed or relaxed (for each isophote) the coordinates of the center of the fitting ellipses and the possibility to complete the masked parts of the isophotes by using the corresponding symmetric parts of the same isophotes with respect to the center.

3.2. Extraction of profiles and error estimates

Once the isophotes have been carefully masked and interpolated through ellipses, we obtained luminosity and geometrical profiles of all galaxies in our sample. In particular, we obtained surface brightness, ellipticity, position angle and coefficients of the Fourier analysis of the residuals as a function of the semi-major axes of the fitted isophote.

The most important contribution to the uncertainties in the outer profiles of nearby elliptical galaxies from CCD data is usually given by the possible errors in the estimate of the background. In particular, an underestimation (overestimation) of the average background level leads to a systematic distortion upwards (downwards) of the outer luminosity profiles and then to an overestimation (underestimation) of the total apparent luminosity. In our case this kind of uncertainty is not the dominant one since the average value of the background is very carefully estimated (well outside the faint galaxy halos) by the above mentioned '*local refinement*'. A more serious problem is represented by the possible systematicity of the background residuals. Fasano and Bonoli (1990) analyzed the influence of an artificially tilted background on the luminosity and geometrical profiles, giving a set of formulae to estimate error bars of surface brightness, ellipticity and position angle of each isophote, mainly depending on the relative background variation (0.5% in our case; see previous subsection) and on the considered isophotal level. Error bars of our profiles were computed according to these formulae, with an additional term (which could be relevant for the outer isophotes) accounting for the number of points belonging to each isophote. This term turns out to be usually negligible for ground-based surface photometries, where the small signal to noise ratio of the outermost regions is largely compensated for the great number of points defining the isophotes. In our case, the incredible depthness and resolution of the images allowed us to perform the

detailed surface photometry of galaxies in which even the outermost isophotes are defined by a relatively small number of points.

4. Results

The profiles of surface brightness (μ), ellipticity (ε), position angle (θ) and coefficient of the Fourier analysis of the residuals (c_4), as a function of the semi-major axis a in arcseconds ($a^{1/4}$ scale), are shown at the end of the paper in Figure 1, together with the proper error bars (see previous Section). In the same figures we report for comparison the *PSF* profile as a dotted line.

4.1. Statistical properties of profiles

4.1.1. Luminosity profiles

We divided our galaxy sample in 3 different classes, according to the luminosity profiles:

- most of galaxies (55) have luminosity profiles following reasonably well the de Vaucouleurs law up to the innermost isophote not significantly affected by the *PSF* (hereafter '*Normal*' class);
- a relevant fraction of galaxies (36), even following the de Vaucouleurs law in the main body light distribution, exhibit in the inner regions a substantial flattening of the luminosity profiles, not attributable to the *PSF* (hereafter '*Flat*' class);
- finally, the isophotal analysis allowed us to detect 8 galaxies showing complex inner structures (most of them are multi-nucleus objects), but still obeying the de Vaucouleurs law in the outer profiles (hereafter '*Merger*' class).

In column (6) of Table 1 the luminosity profile class of each galaxy is reported and the three classes are indicated with 1, 2 and 3, respectively. The same convention is used in Table 2.

Concerning the '*Flat*' class, it is worth stressing that the observed inward flattening of the luminosity profiles with respect to the de Vaucouleurs law cannot be interpreted as due to the presence of some *core*-like structure. Actually, in all galaxies of this class for which the redshift has been measured (6 objects), the linear size of the involved regions turns out to be much greater than the typical *core* size (10^2 *pcs*). For instance, at $z \sim 1$, 10^2 *pcs* correspond to $\sim 0.^{\circ}01$, with small differences in the range $0.5 \leq z \leq 3$. On the other hand, galaxies with luminosity profile flattening confined inside $\sim 0.^{\circ}1$ have been included by default in the '*Normal*' class. Moreover, by comparing the fraction of HDF ellipticals belonging to the '*Flat*' class with that obtained in a similar way from the sample of local ellipticals provided by Djorgovski (1985), we found a relevant difference in favour of the HDF sample ($\sim 36\%$ vs. $\sim 7\%$). We will see in a forthcoming paper (Fasano et al. 1997) that the different classes of luminosity profiles are often associated with different physical properties of the galaxies (i.e. colors and sizes).

Finally, we mention that the luminosity profile of the galaxy *ID_2.251.0* strongly suggests the presence of a nuclear point source. This galaxy also belongs to the lists of radio and ISO sources in the HDF (Fomalont et al. 1997, Mann et al. 1997).

4.1.2. Ellipticity profiles

The shape of the ellipticity profiles appears to be correlated with the above mentioned luminosity profile classes. Actually, the galaxies belonging to the ‘Normal’ class show increasing or almost constant ellipticity profiles (see Fig.1). This is the most common behaviour in nearby early-type galaxies (see Bettoni et al. 1996). On the other hand, 25 out of the 44 galaxies belonging to the ‘Flat’ class or to the ‘Merger’ class show strongly decreasing ellipticity profiles (see Fig.1). This is an unusual behaviour in the local samples of early-type galaxy (Bettoni et al. 1996). Table 2 reports some statistical data on the shapes of the ellipticity profiles.

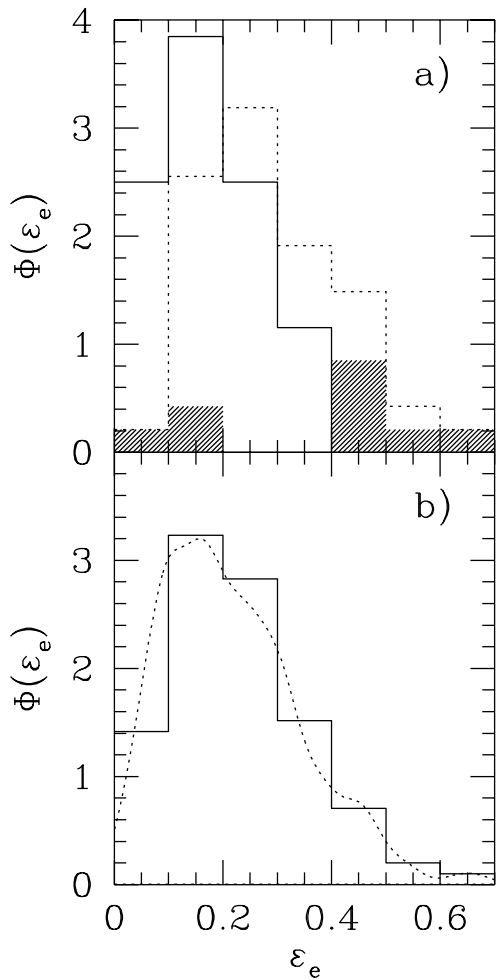


Fig. 2. a) effective ellipticity distribution of the ‘Normal’ galaxies (full line histogram) compared with that of ‘Flat+Merger’ (dotted histogram). The shaded histogram refer to the ‘Merger’ class alone. b) effective ellipticity distribution of the total sample (full line histogram) compared with that of ‘local’ sample from the literature (Fasano and Vio 1991).

This peculiarity of the ellipticity profiles is likely to reflect

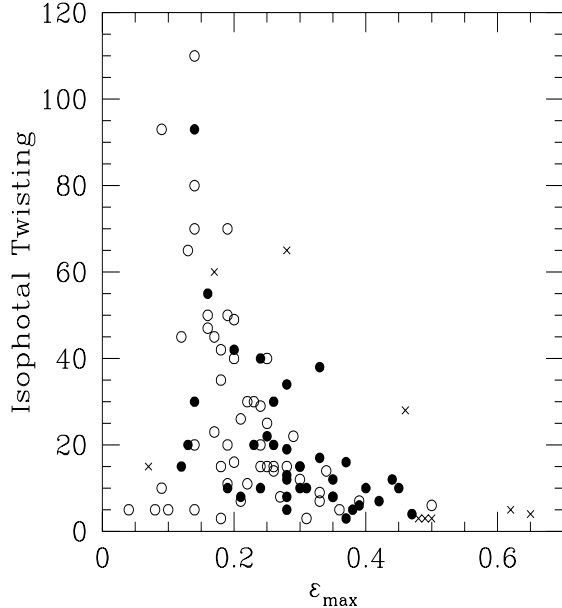


Fig. 3. Maximum ellipticity vs. isophotal twisting (open circles: ‘Normal’ class; full circles: ‘Flat’ class; crosses: ‘Merger’ class).

on the ellipticity distribution (computed at the effective radius, see column 9 of Table 1) of galaxies in our sample. Figure 2a shows that the ellipticity distribution of the ‘Normal’ class looks remarkably different from that relative to the other two classes, the last ones being shifted towards flatter configurations. The Kolmogorov-Smirnov test confirms this difference at high significance level (98.5%). Nevertheless, the ellipticity distribution of the whole sample (Figure 2b) seems to be in fair agreement with that relative to nearby galaxy samples (see Fasano and Vio 1991). It is worth stressing that the comparison with the local samples is not invalidated by the fact that the selection criteria of our sample extend to the limit of recognition between stars and galaxies. In fact the error bars shown in the ellipticity profiles take into account the influence of the PSF (see Section 3.2).

4.1.3. Isophotal shape and twisting

In Table 2 we report some statistics on the shape of the isophotes (‘disky’ for $c_4 > 0$; ‘boxy’ for $c_4 < 0$) in our galaxy sample for the different luminosity profile classes. There is a weak indication than the fraction of *boxy* galaxies increases from the ‘Normal’ to the ‘Flat’ and ‘Merger’ classes.

Concerning the position angle profiles, although the uncertainties involved in measuring the position angle of outer isophotes are relevant for HDF ellipticals, we estimate that the amount of isophotal twisting in our sample is larger (on average) than that found in local galaxy samples (see Fasano and Bonoli 1989). This fact may be explained as a consequence of the high fraction of morphologically perturbed objects in the HDF.

Figure 3 shows the distribution of HDF early-type galaxies in the ‘maximum ellipticity - twisting’ plane, which, even being qualitatively similar to that of local samples (see Gal-

letta 1980), shows an higher fraction of significantly twisted objects. The maximum ellipticity ε_{max} and the total isophotal twisting (in degrees) are reported in columns (10) and (11) of Table 1, respectively.

Table 2. Statistical Properties of profiles

Class	1	2	3	All
average ellipticities				
$\langle \varepsilon_e \rangle$	0.17	0.28	0.38	0.23
$\langle \varepsilon_{max} \rangle$	0.21	0.30	0.40	0.26
ellipticity profiles (%)				
$\varepsilon \nearrow$	36	14	0	25
$\varepsilon \sim$	58	33	22	46
$\varepsilon \searrow$	6	53	75	29
isophotal shape (%)				
<i>disky</i>	33	25	11	28
<i>elliptical</i>	14	11	0	12
<i>boxy</i>	22	33	50	29
<i>irregular</i>	31	31	33	31
#gal.	55	36	8	99

4.2. Extraction of the global parameters

In order to derive total magnitudes and half-light radii of the galaxies, it is convenient to use some analytical representation of the luminosity profiles. This allows a suitable smoothing of each profile and provides an easy way to extrapolate it. For obvious reasons it is also convenient to operate on the ‘equivalent’ luminosity profiles, that is to multiply the semi-major axis (a) by the factor $\sqrt{1 - \varepsilon(a)}$.

The most common technique to get suitably smooth representations of any observed function is the bicubic-spline interpolation. In the case of luminosity profiles of elliptical galaxies, a nice representation is also given by the Sersic function (1968, see also Ciotti 1991). However, we preferred to represent the equivalent luminosity profiles by means of sums of gaussian functions whose peak intensities regularly decrease at increasing the standard deviations (multi-gaussian expansion technique). In a forthcoming paper (Fasano et al. 1997) we will see that this representation is useful to perform the deconvolution of the luminosity profiles (Bendinelli 1991, Emsellem et al. 1994). Here we wish only to mention that, in our particular case, this method gives usually a better representation with respect to the bicubic-spline method, especially in the inner part of luminosity profiles.

The multi-gaussian representation was also used to extrapolate the profiles. In general, it was forced to follow the de Vaucouleurs law down to very faint values of μ . However, if the galaxy size is comparable with the PSF size (very steep profiles), it is necessary to impose that the multi-gaussian extrapolation of the outer galaxy profile does not fall below the very extended wings of the *HST-PSF* itself. To this end we forced the extrapolation of the luminosity profiles of very small galaxies to converge smoothly towards the PSF profile at large radii. Luminosity profiles with an effective radius larger than three times the *FWHM* were extrapolated simply by a de Vaucouleurs’ law.

A special warning is needed when computing the total magnitude of galaxies belonging to the above defined ‘Merger’ class,

since their complex inner structures make undefined (or unreliable) the inner part of luminosity profiles. In these cases the flux inside the innermost reliable ellipse was directly measured on the frame and was considered as an additional contribution to the integral of the luminosity profile, computed from that ellipse and extrapolated by a de Vaucouleurs law. The total magnitudes in the V_{606} band (*STMAG* system) and the corresponding equivalent effective (half-light) radii r_e are reported in the columns (7) and (8) of Table 1, respectively. The quantities in brackets close to the column (7) represent the surplus magnitudes Δ_m due to the extrapolation procedure. They give an indication of the quality of the total magnitude estimates. Adding these quantities to V_{606}^{Tot} one obtain, for each galaxy, the magnitude before extrapolation.

In Figure 4 we compare the V_{606} -*STMAG* total magnitudes from our detailed surface photometry with the automated *FOCAS* magnitudes given by Williams et al. (1996), corrected for the average offset of $0^m.2$ between the *ABMAG* and the *STMAG* systems. There are two galaxies (*ID_2_726_1* and *ID_4_289_0*) for which the flux has been probably overestimated by *FOCAS*, due to the presence of very close companions. Apart from these cases, the total fluxes computed with our procedure tend to be systematically greater than those obtained with the automated photometry. Moreover, the difference increases at increasing both the average surface brightness of the galaxies and (weakly) their angular size. This fact is not surprising and it is likely to indicate that the automated photometry tends to underestimate the halos of the ellipticals. To this concern, it is also worth noticing that the differences ΔV_{mag} in Figure 4 turn out to be roughly proportional to the previously mentioned quantities Δ_m .

References

- Bendinelli O., 1991, ApJ, 366, 599
- Bertin E., Arnouts S., 1996, A&AS, 117, 393
- Bettoni D., Fasano G., Kjaergaard P. and Moles M. 1996, Second Stromlo Symposium: *The Nature of Elliptical Galaxies*, ASP Conference Series, 116, 71
- Chiosi, C., Bressan, A., Portinari, L. and Tantalo, R., 1997, A&A, submitted, babbage astro-ph/9708123
- Ciotti L. 1991, A&A 249, 99
- Couch W.J., 1996, <http://ecf.hq.eso.org/hdf/catalogs/>
- Djorgovski, S., 1985, Ph.D. Thesis, University of California, Berkeley
- Djorgovski, S., Davis, M. 1987, ApJ, 313, 59
- Dressler, A., Lynden-Bell, D., Burstein, D., Davies, R. L., Faber, S. M., Terlevich, R. J., Wegner, G. 1987, ApJ, 313, 42
- Ellis, R.S., 1997, Proc. of the STScI May Symposium: *The Hubble Deep Field*, babbage astro-ph/9708075
- Emsellem, E., Monnet, G., Bacon, R. 1994, A&A, 285, 723
- Fasano G. 1990, internal report of the Padova Astronomical Observatory
- Fasano G. and Bonoli C. 1989, A&AS, 79, 291
- Fasano G. and Bonoli C. 1990, A&A 234, 89
- Fasano G. and Vio R. 1991, MNRAS, 249, 208
- Fasano G., Cristiani S., Arnouts S. and Filippi M. 1997, AJ, submitted
- Filippi M., Fasano G., Bertola F. 1997, in preparation
- Fomalont E.B., Kellermann K.I., Richards E.A., Windhorst R.A. and Partridge R.B. 1997, ApJ, 475, L5

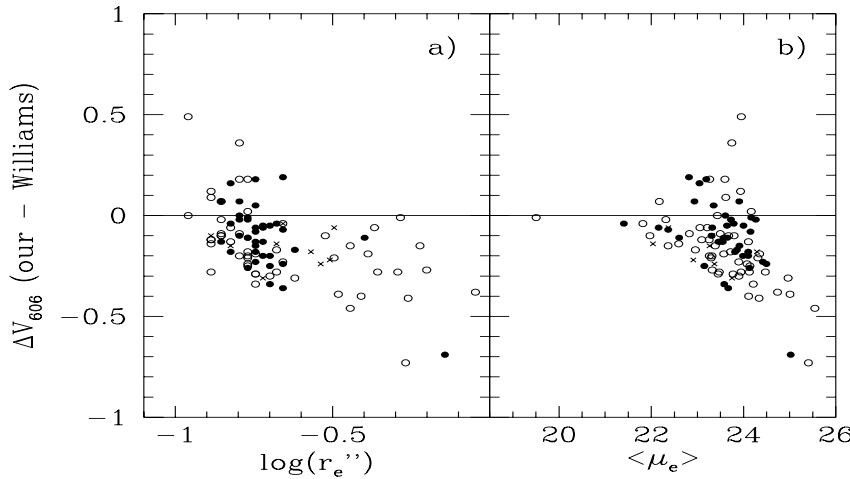


Fig. 4. Difference between our total magnitudes and the magnitudes given by Williams et al. (1996) as a function of the effective radius (panel a) and of the average surface brightness (panel b). The meaning of the symbols is the same as in Fig.3.

- Galletta G. 1980, A&A, 181, 179
 Giavalisco, M., Steidel, C.C. and Macchetto, F.D., 1996, ApJ, 470, 189
 Kauffmann G., Charlot S., 1997, submitted to MNRAS, babbage astro-ph/9704148
 Jenkins, A., Frenk, C.S., Pearce, F.R., Thomas, P.A., Colberg, J.M., White, S.D.M., Couchman, H.M.P., Peacock, J.A., Efstathiou, G. and Nelson, A.H., 1997, ApJ, submitted, babbage astro-ph/9709010
 Lowenthal, J.D., Koo, D.C., Guzman, R., Gallego, J., Phillips, A.C., Faber, S.M., Vogt, N.P., Illingworth, G.D. and Gronwall, C., 1997, ApJ, 481, L673
 Madau, P., Pozzetti, L. and Dickinson, M., 1997, ApJ, submitted, babbage astro-ph/9708220
 Mann, B. et al. (The ISO-HDF Consortium) 1997, MNRAS, submitted
 Oemler, A.Jr., Dressler, A. and Butcher, H.R., 1997, ApJ, 474, 561
 Pettini, M., Steidel, C.C., Dickinson, M., Kellogg, M., Giavalisco, M. and Adelberger, K.L., 1997, Proc. of the meeting: *The Ultraviolet Universe at Low and High Redshift*, ed. W. Waller, (Woodbury: AIP Press), babbage astro-ph/9707200
 Sersic, J.L. 1968, ‘*Atlas de galaxias australes*’, Observatorio Astronomico de Cordoba, Argentina
 Shade, D., Carlberg, R.G., Yee, H.K.C., Lopez-Cruz, O. and Ellingson, E., 1996, ApJ, 464, L63
 Shade, D., Barrientos, L.F. and Lopez-Cruz, O., 1997, ApJ, 477, L20
 Statler T., 1996, private communication
 Tantalo R., Chiosi C., Bressan A., Fagotto F., 1996, A&A 311, 361
 Tully, R.B., Fisher, J.R.T., 1977, A&A 54, 661
 van den Bergh S., Abraham R.G., Ellis R.S., Tanvir N.R., Santiago B.X., Glazebrook K.G., 1996, AJ 112, 359
 van Dokkum, P.G. and Franx, M., 1996, MNRAS, 281, 985
 White, S.D.M., 1997, Proc. of the 3rd ESO-VLT Workshop: *Galaxy Scaling Relations: Origins, Evolution and Applications*
 Williams R. E., Blacker B., Dickinson M., Dixon W., Ferguson H. C., Fruchter A. S., Giavalisco M., Gilliland R. L., Heyer I., Katsanis R., Levay Z., Lucas R. A., McElroy D. B., Petro L., Postman M., 1996, AJ, 112, 1335

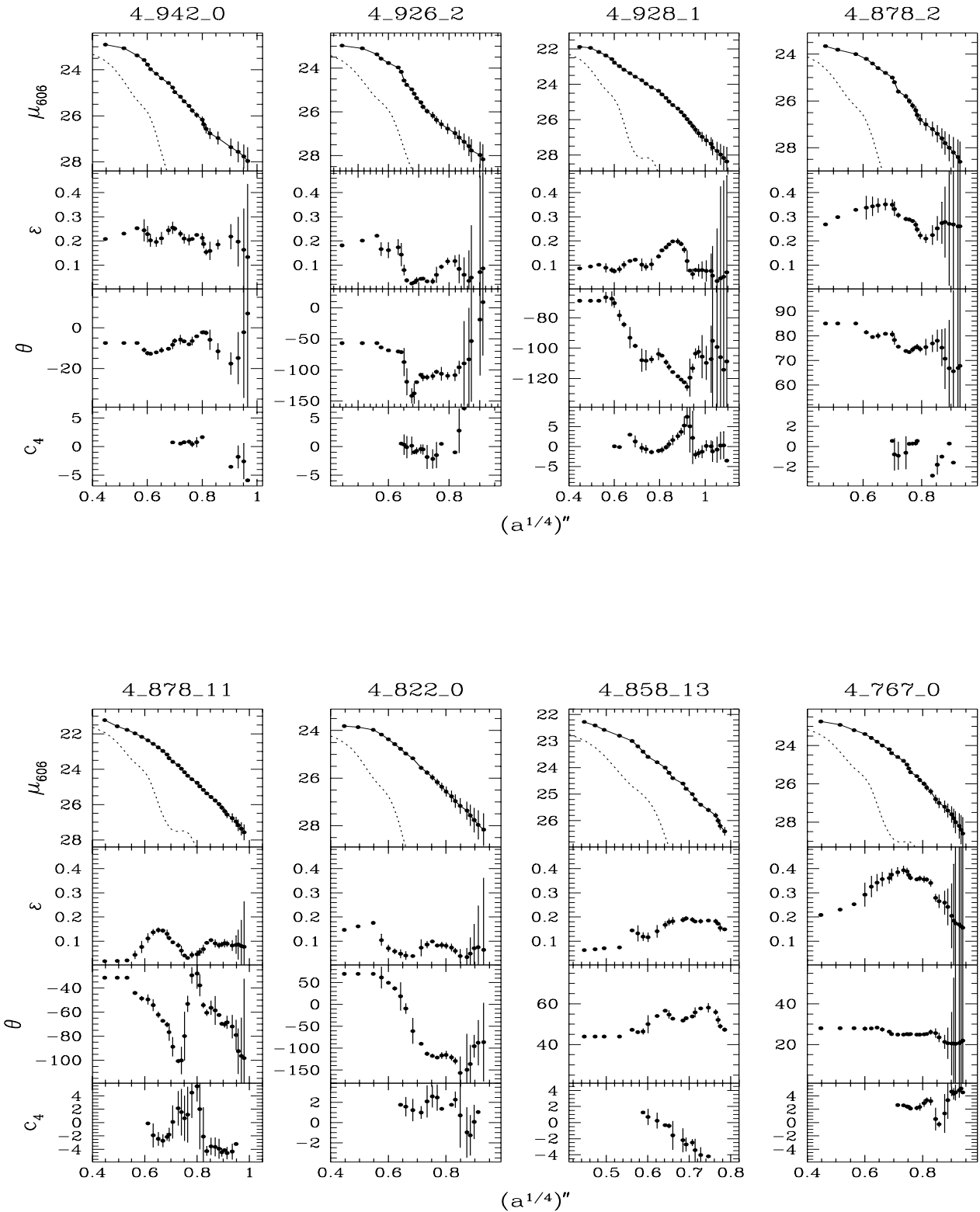


Fig. 1. Luminosity and geometrical profiles of elliptical galaxies in the HDF

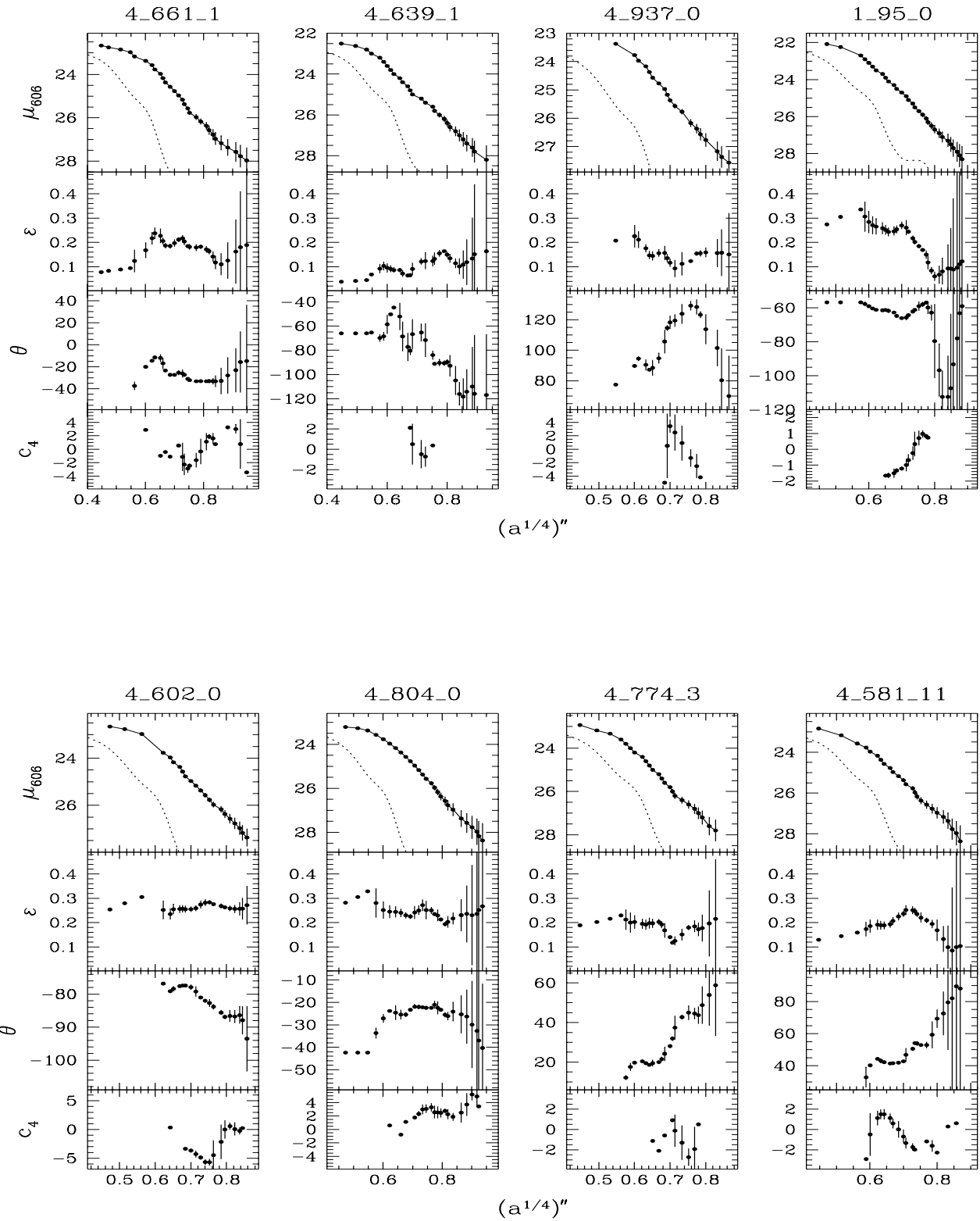


Fig. 1. ...continue...

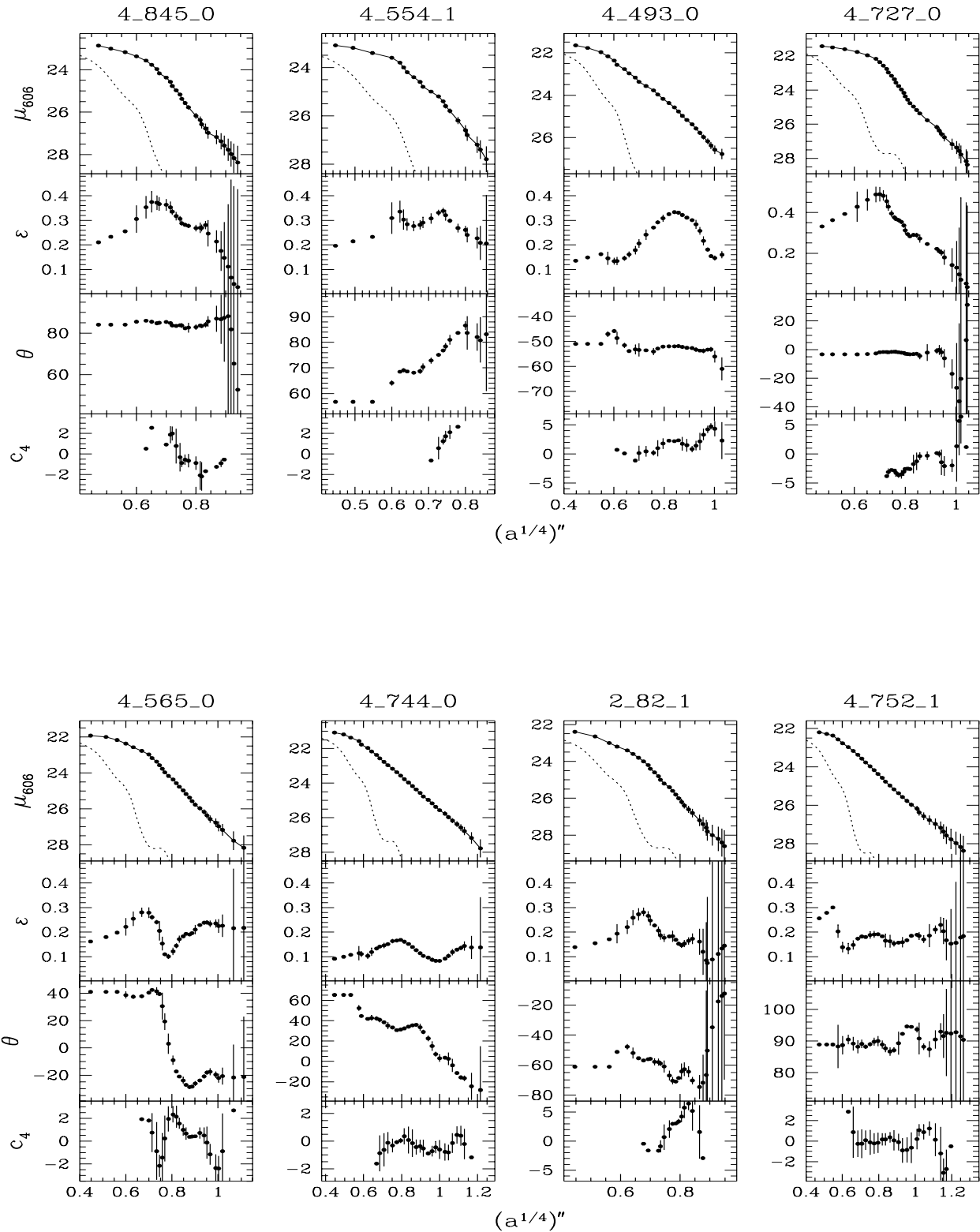


Fig. 1. ...continue...

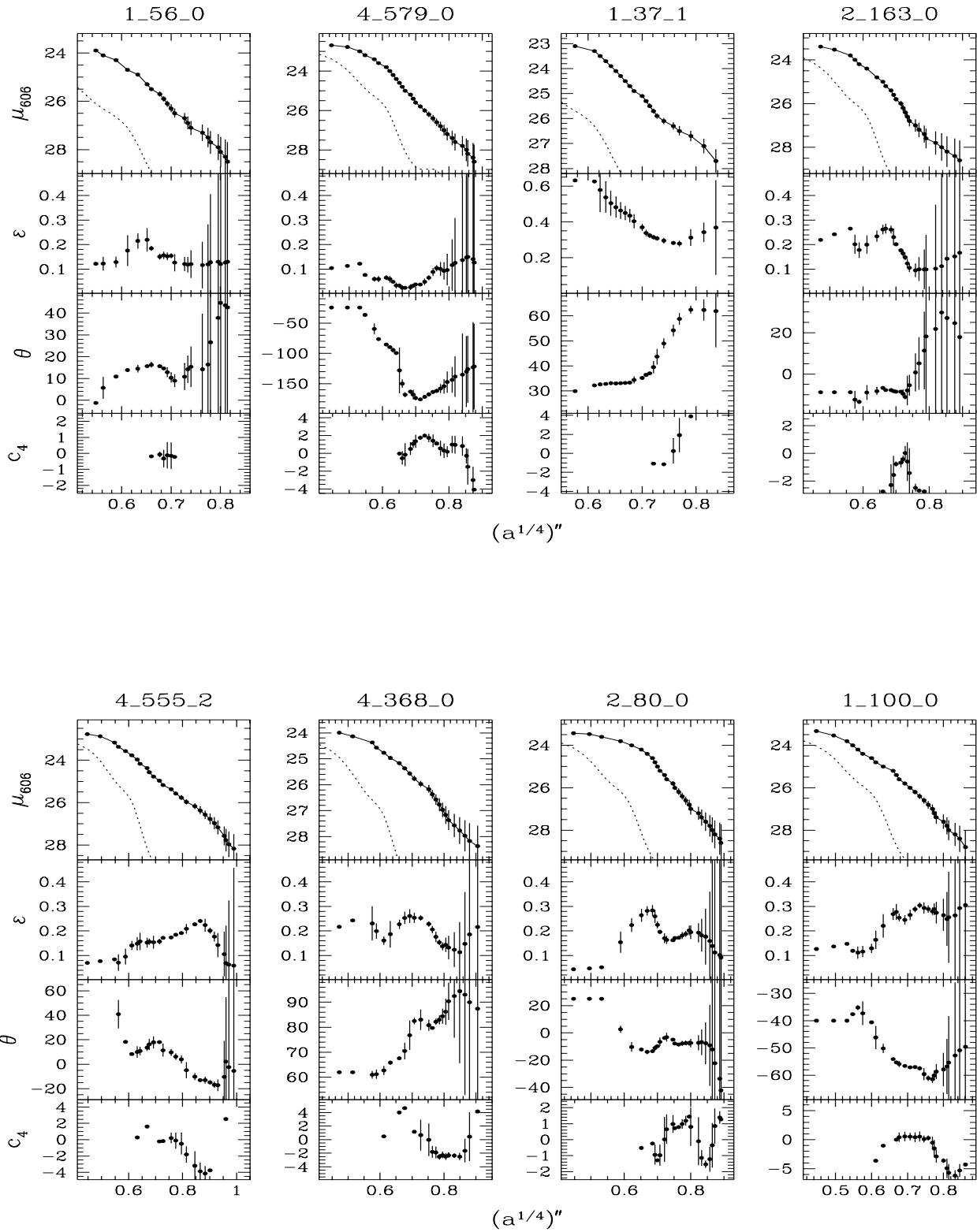


Fig. 1. ...continue...

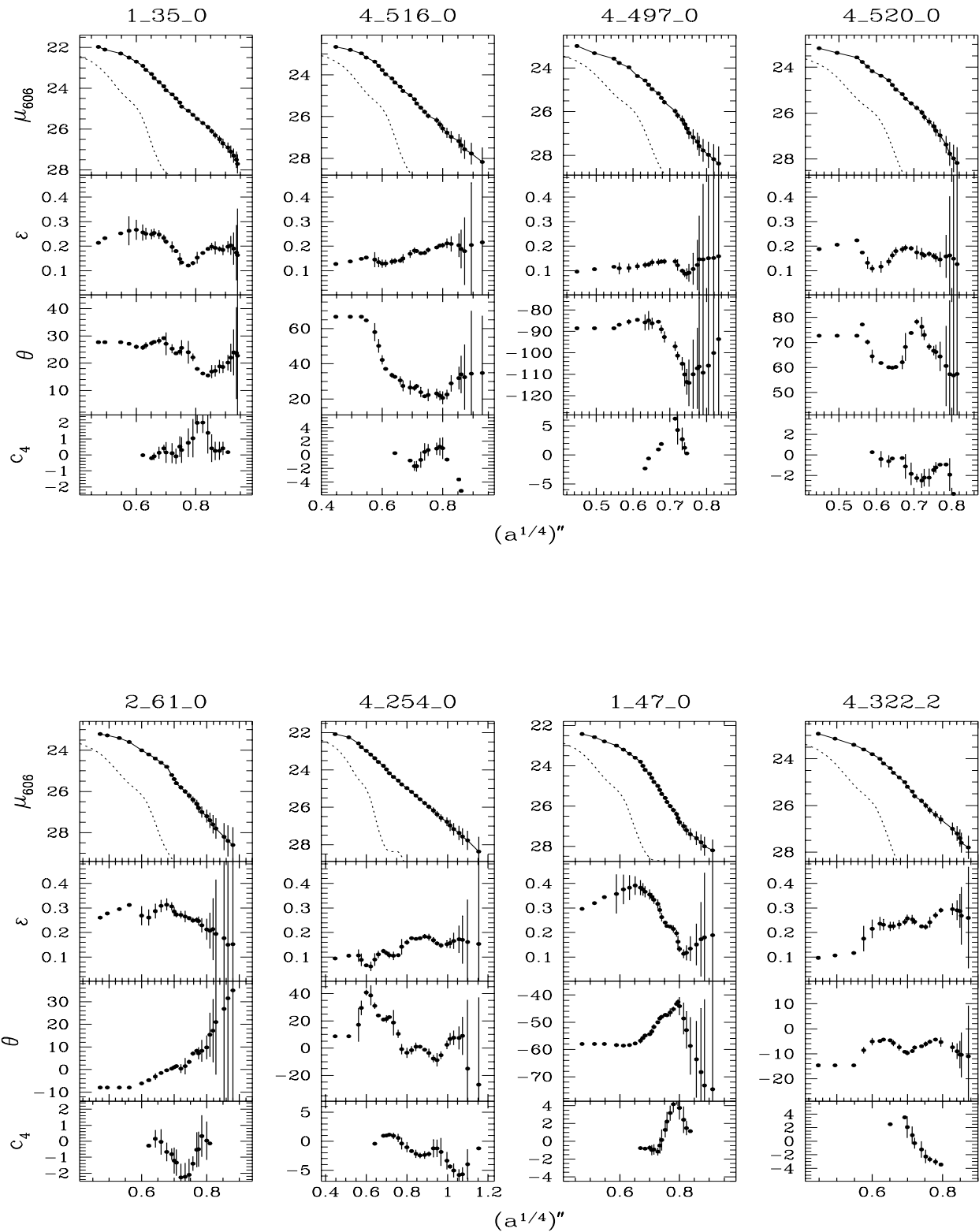


Fig. 1. ...continue...

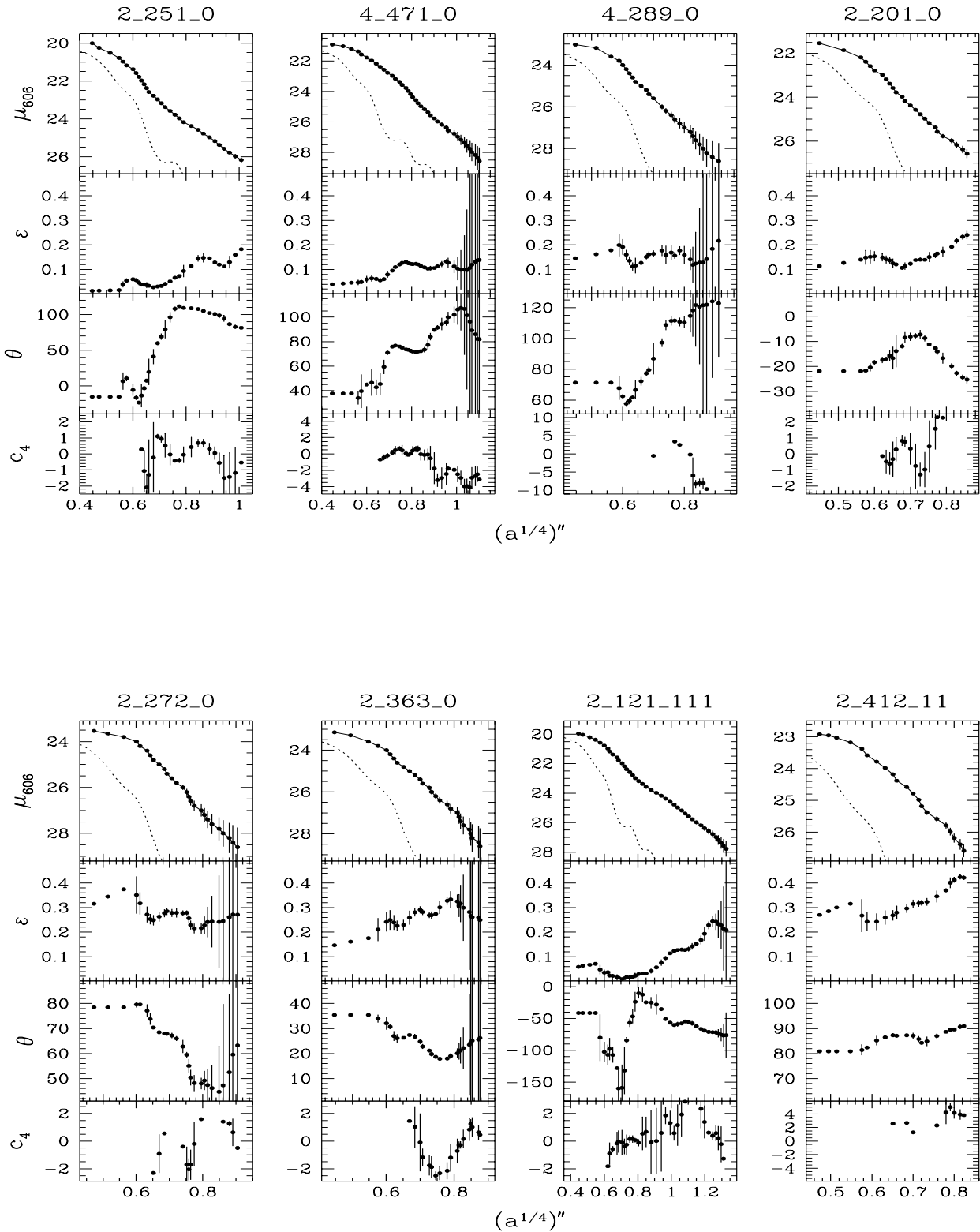


Fig. 1. ...continue...

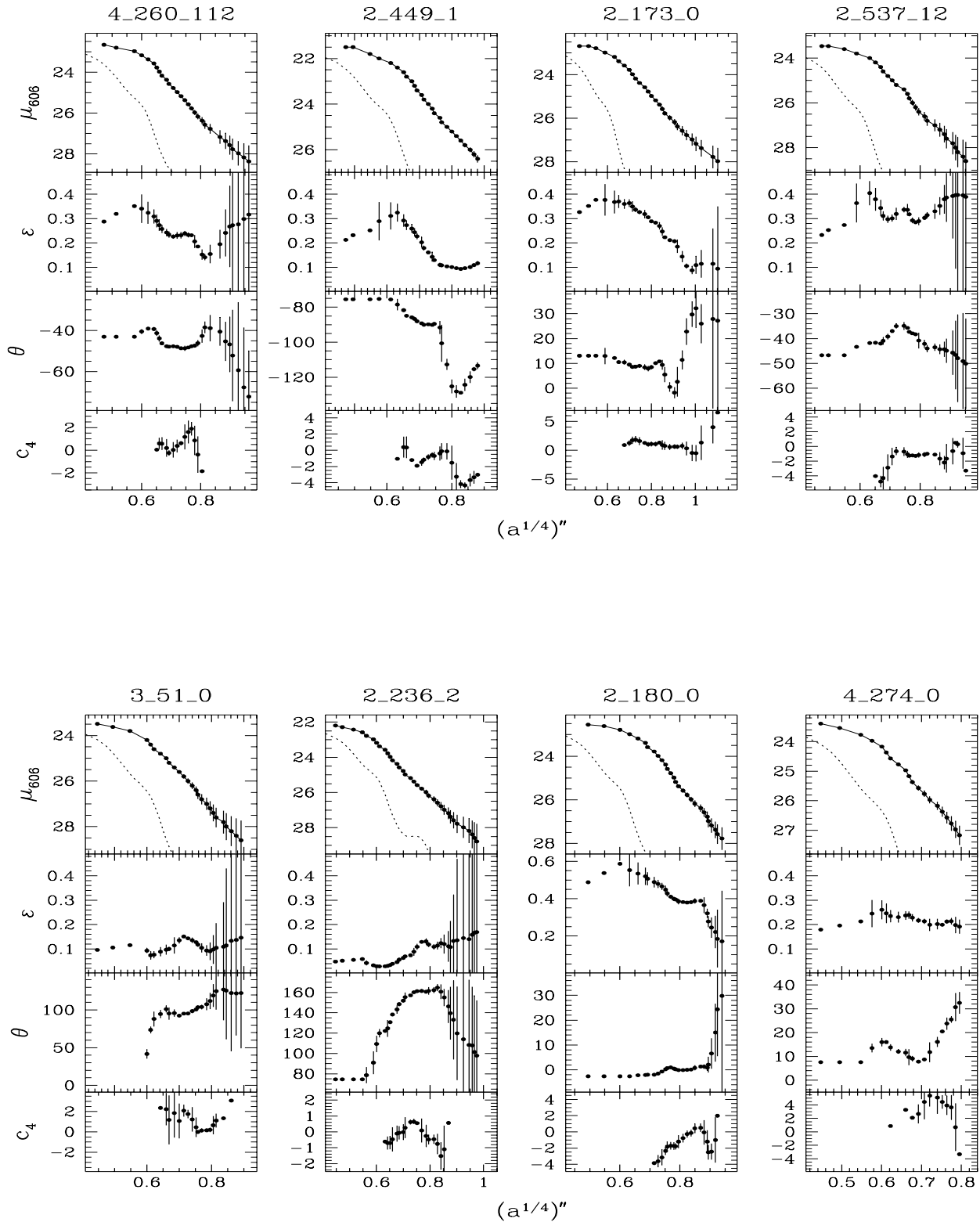
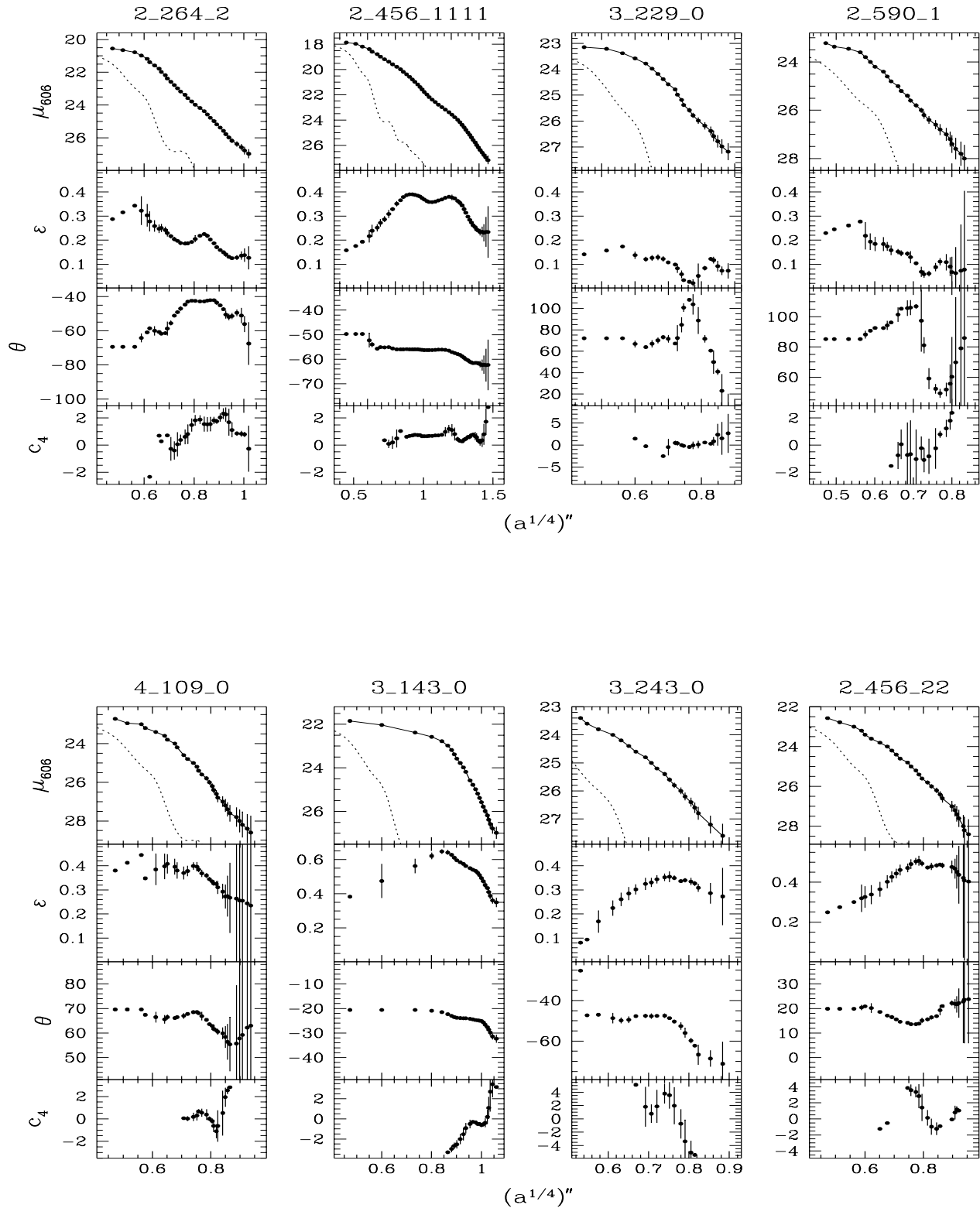


Fig. 1. ...continue...

**Fig. 1.** ...continue...

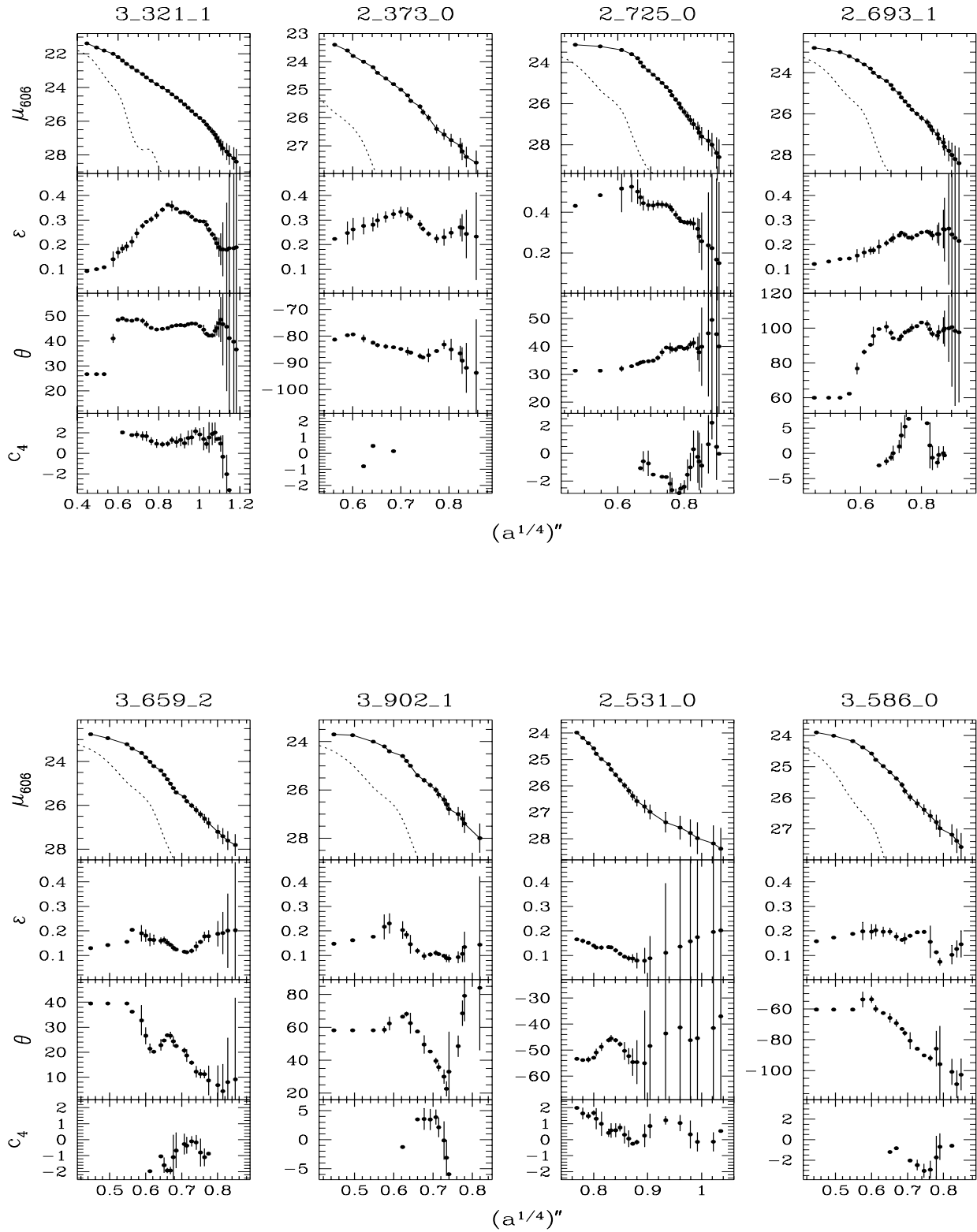


Fig. 1. ...continue...

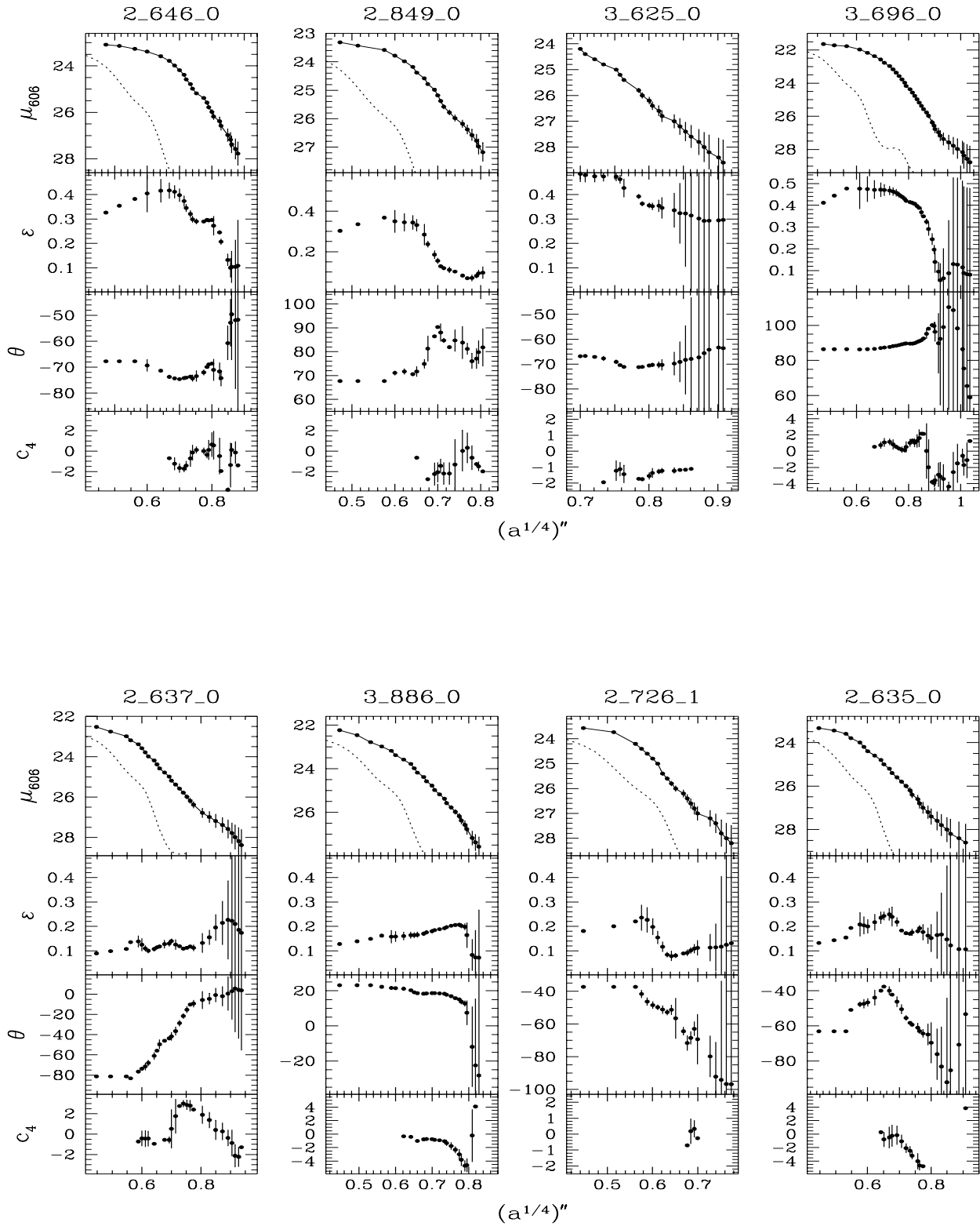


Fig. 1. ...continue...

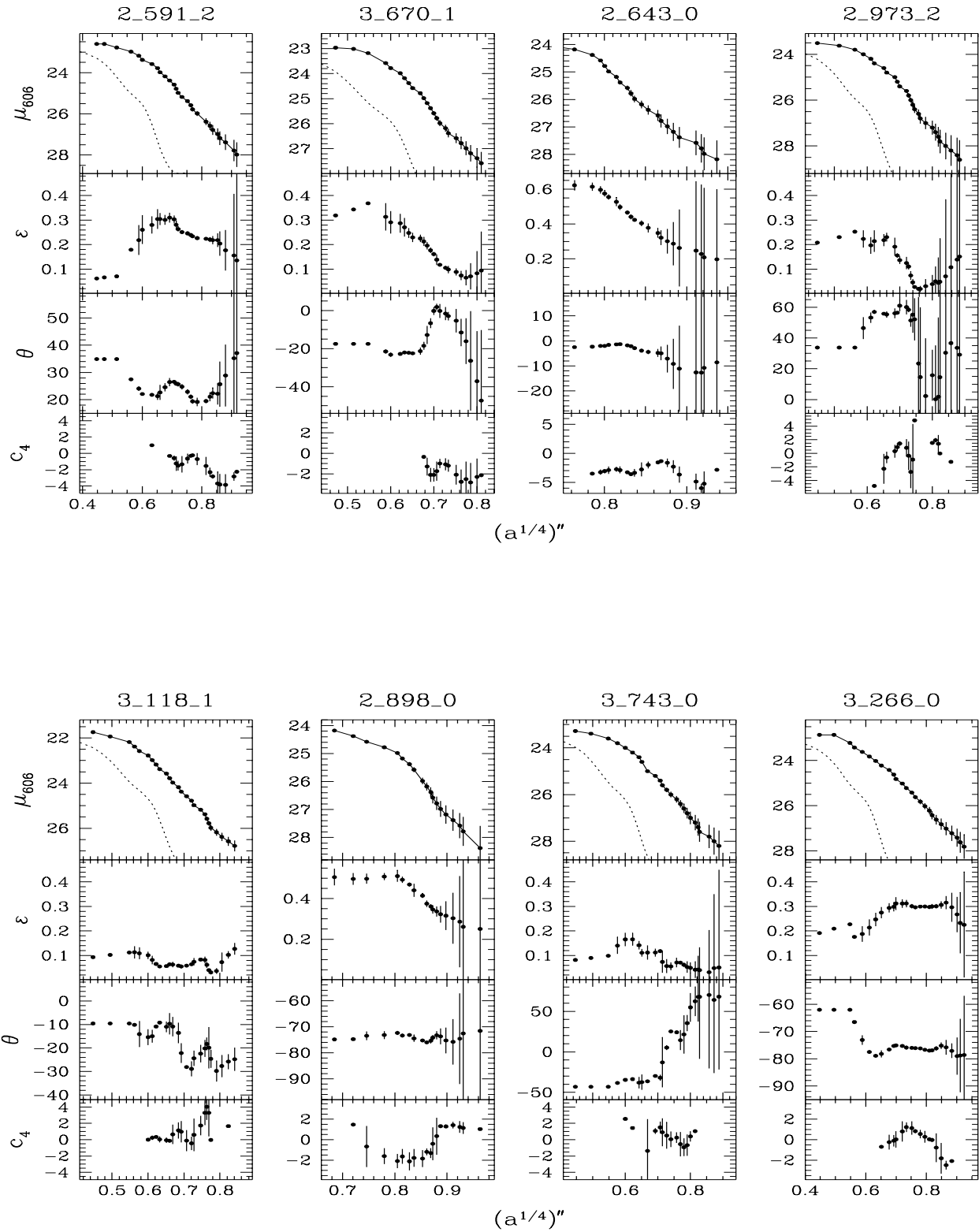


Fig. 1. ...continue...

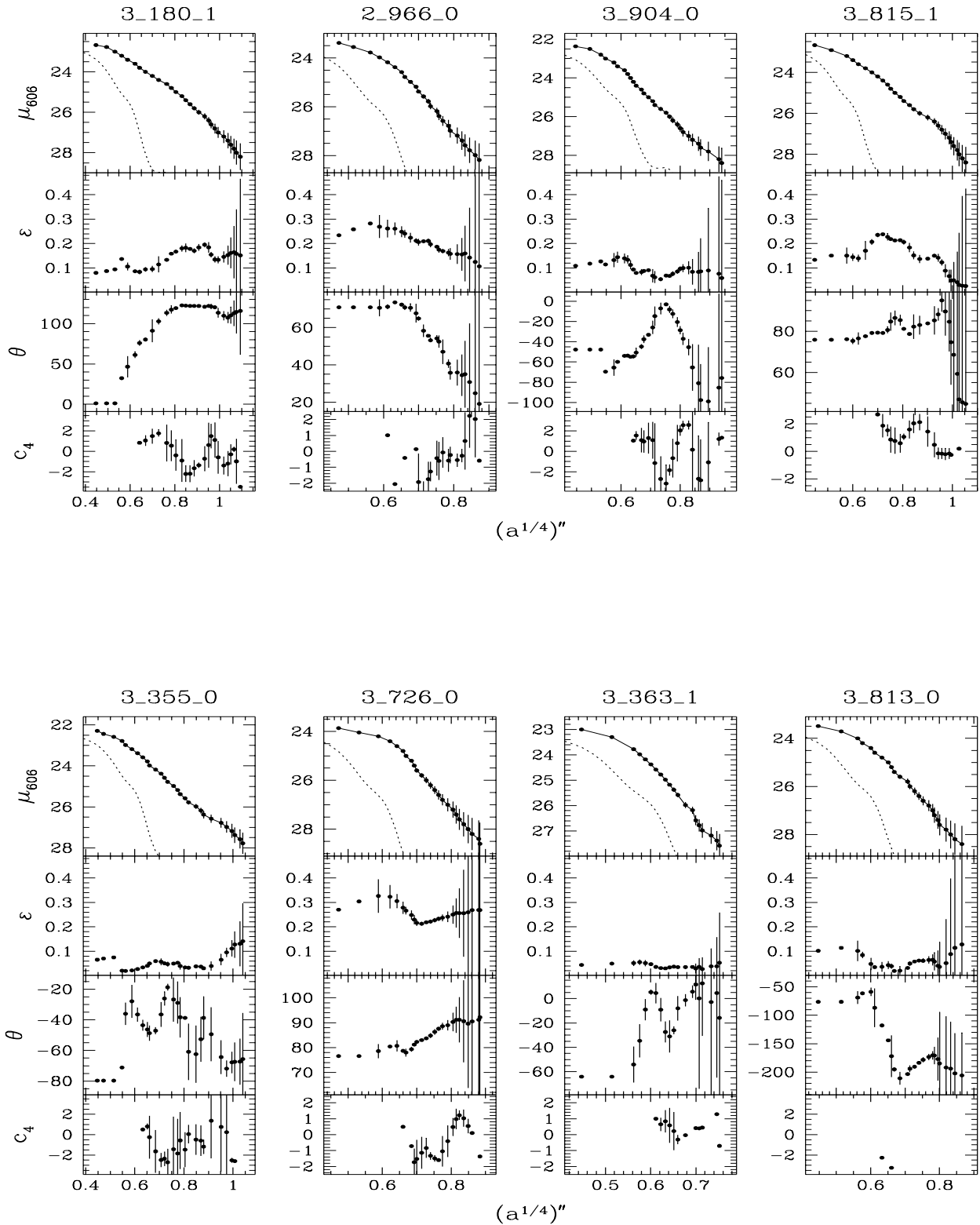


Fig. 1. ...continue...

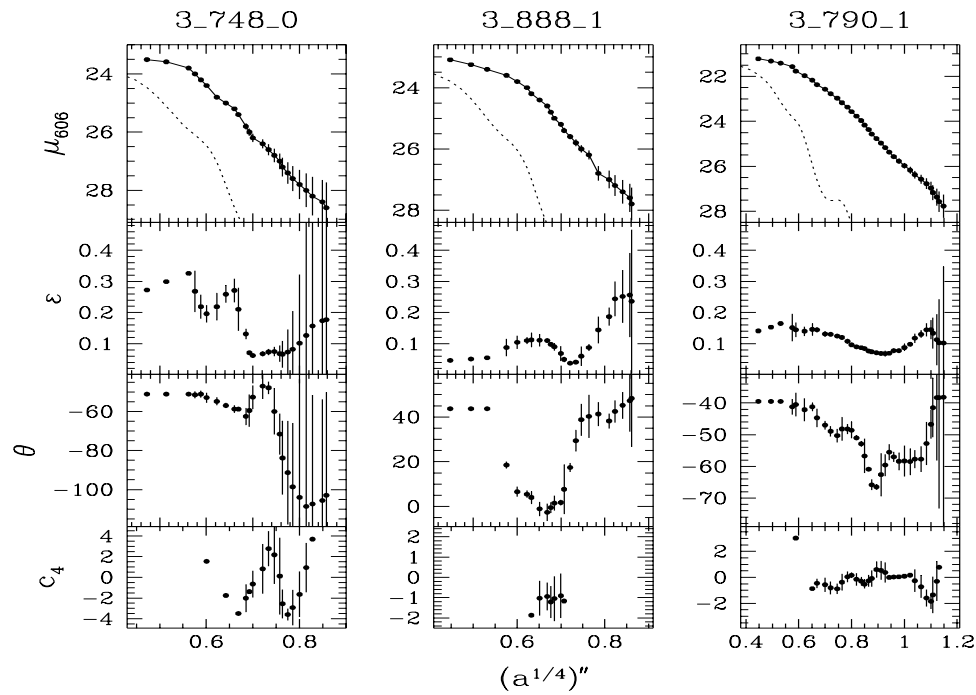


Fig. 1. ...continue

This article was processed by the author using Springer-Verlag L^AT_EX
A&A style file 1990.